Watermarked cardiac CT image segmentation using deformable models and the Hermite transform

Sandra L. Gomez-Coronel[a,b], Ernesto Moya-Albor[c],
Boris Escalante-Ramírez[a] and Jorge Brieva[c];

[a] Fac. de Ingeniería, Universidad Nacional Autónoma de México, México, D.F.
[b] Instituto Politécnico Nacional, UPIITA, Av. IPN No. 2580 Col. La Laguna Ticomán, Gustavo A. Madero, México D.F. C.P. 07340
[c] Fac. de Ingeniería, Universidad Panamericana, México, D.F.

ABSTRACT

Medical image watermarking is an open area for research and is a solution for the protection of copyright and intellectual property. One of the main challenges of this problem is that the marked images should not differ perceptually from the original images allowing a correct diagnosis and authentication. Furthermore, we also aim at obtaining watermarked images with very little numerical distortion so that computer vision tasks such as segmentation of important anatomical structures do not be impaired or affected.

We propose a preliminary watermarking application in cardiac CT images based on a perceptive approach that includes a brightness model to generate a perceptive mask and identify the image regions where the watermark detection becomes a difficult task for the human eye. We propose a normalization scheme of the image in order to improve robustness against geometric attacks. We follow a spread spectrum technique to insert an alphanumeric code, such as patient's information, within the watermark. The watermark scheme is based on the Hermite transform as a bio-inspired image representation model.

In order to evaluate the numerical integrity of the image data after watermarking, we perform a segmentation task based on deformable models. The segmentation technique is based on a vector-value level sets method such that, given a curve in a specific image, and subject to some constraints, the curve can evolve in order to detect objects. In order to stimulate the curve evolution we introduce simultaneously some image features like the gray level and the steered Hermite coefficients as texture descriptors.

Segmentation performance was assessed by means of the Dice index and the Hausdorff distance. We tested different mark sizes and different insertion schemes on images that were later segmented either automatic or manual by physicians.

Keywords: Perceptive watermarking, Hermite transform, deformable models, texture segmentation.

1. INTRODUCTION

Digital multimedia and communication system has increased the distribution of medical data in a digital format, because in this way is easy to support diagnosis tasks related to computer tomography images, also it is possible to exchange databases between hospitals. But these advantages have introduced new risks for inappropriate use of medical information, given the ease with which digital content can be manipulated or copied for illegal uses. It is thus necessary to develop security mechanisms that guarantee protection of medical contents, specially their integrity.[1] Medical image watermarking is an open area for research and is a subcategory of image watermarking that is a solution for the protection of copyright and intellectual property.[2] Watermarking in digital images consists of embedding information into the code related to the author or copyright holder. The quality of a

Send correspondence to E.M.A.
E.M.A.: E–mail: emoya@up.edu.mx, Telephone: +52 55 5482 1600 Ext. 5210
S.L.G.C.: E–mail: sgomezc@ipn.mx,
B.E.R.: E-mail: boris@servidor.unam.mx,
J.B.: E-mail: jbrieva@up.edu.mx

10th International Symposium on Medical Information Processing and Analysis,
edited by Eduardo Romero, Natasha Lepore, Proc. of SPIE Vol. 9287, 928717

watermarking technique and the corresponding resultant image is measured in terms of robustness, legibility, imperceptibility, and ambiguity.[3] In the case of medical images, watermarking has been proposed as a mechanism to improve their security. In this area is important to take account that images have special requirements, i.e., watermarked images should not differ perceptually from their original, because the clinical reading of the images must not be affected. Also reversibility of the watermarking algorithm is an important requirement to ensure lossless detection of both host image and the watermark at destination for correct diagnosis and authentication.[4] The watermark can be patient's information, patient's code number, doctor's number code, etc., and it is important to take account robustness and imperceptibility aspects, because robustness implies introducing stronger image distortions that compromise the watermark imperceptibility and the perceptual changes in the original medical image. There are many medical application scenarios for digital watermarking:

1. Integrity control, to verify that the image has not been modified without authorization, in order to preserve their diagnostic value.
2. Authenticity, that is to verify that the image is really what the user supposes it is.
3. Access control, digital watermarking provides an efficient access control mechanism and enforces medical confidentiality protection, by embedding patients personal/examination data into medical images.
4. Indexing, digital watermarking has the potential of being an alternative for indexing, archiving, and managing medical data in hospital information systems. Watermarks can play the role of keywords, based on which efficient archiving and easy data retrieval from querying mechanisms can take place.

Many watermark systems have been developed either in the spatial domain and the transform domain. In the spatial domain[5–7] the watermark is embedded into the LSBs (Least Significant Bits) of the original image. But the inserted information maybe easily detected and modified using computing analysis, so this technique is not robust and rarely survives various attacks. In the transform domain the watermark is embedded into the transform coefficients of the original image. Transforms most used are the Discrete Fourier Transform (DFT), the Discrete Wavelet Transform (DWT), the Discrete Cosine Transform (DCT), the Contourlet Transform.[8–11] Some models use the Human Vision System (HVS) characteristics in order to obtain good results of imperceptibility and robustness, taking advantage of the sensitivity of frequency, luminance and masking contrast. A watermark that exploits the perceptual information is named a perceptual watermark.[10,11] Transform domain techniques that use perceptual masks based on HVS properties have proved to be more robust since they resist geometric and filter attacks. In the medical area different watermarking scheme has been proposed. For example Wu et al[12] proposed a scheme that divides an image into blocks and each block is embedded with the authentication message and the recovery information of other blocks. In this scheme is carried out tampering detection. If tampering is detected, recovery information is extracted from the corresponding block. Also reversible image watermarking algorithms had been proposed.[13,14] Jasni et al.[14] developed a reversible watermarking where hash function is used to protect the ROI (Region of Interest). Hash value of the whole image is embedded in the RONI (Region Of Non Interest) as the watermark. The beauty of ultrasound images and all other medical images is that the LSBs for all pixels in the RONI are zeroes. The watermark is reversed by simply setting the LSBs of RONI back to zero.

In this work we develop a watermarking application in Computed Tomography (CT) cardiac images using the Hermite transform as bio-inspired image model that incorporates a brightness model and a normalization scheme of the image to improve robustness against geometric attacks. Image normalization[15,16] is well known in computer vision and pattern recognition areas. With this process the original image must be transformed into another one in which the orientation and scale of objects in the image are fixed, thus the effects of a geometric attack are minimize. We use a brightness model in order to build a perceptive mask that helps determining the image positions where it is more likely to hide information without producing perceivable artifacts, i.e. this model exploits the limited sensibility of the human visual system to noise detection in areas of high or low brightness. Moreover, we performed a segmentation of left ventricle in order to evaluate how the watermarking algorithm modifies the visual information, as well as the data integrity, and consequently harm the correct diagnosis by physicians. This segmentation is carried out using a deformable model approach that incorporates gray level

and texture image descriptors. For this purpose, we used the steered Hermite coefficients to describe important image structures such as edges and oriented patterns.

The Hermite transform[17,18] is an image representation model that mimics some of the more important properties of early vision such as local processing and the Gaussian derivative models of receptive fields. We used the Hermite transform to embedded the watermark into the transform coefficients of the original image. A rotated version of the Hermite transform provides a very efficient representation of oriented patterns which enables an adaptation to local orientation content at each window position over the image, indicating the direction of one-dimensional pattern. The steered Hermite coefficients were used as texture descriptors in the deformable model to handle the curve evolution and allowing left ventricle segmentation.

We evaluated both watermark and segmentation performances. In the first case we used objective metrics to evaluate the insertion and extraction of the watermark process, and verified that watermarked images do not considerably differ perceptually nor numerically from their originals. For the segmentation algorithm, we used two metrics to compare differences between the segmentation of the original and watermarked images.

This paper is organized as follows: Section 2 is dedicated to introduce the cartesian and steered Hermite transform. In Section 3 the proposal watermarking algorithm is explained. The segmentation method used is reported in Section 4. Section 5 is dedicated to the experiments, where in Section 5.2 we present results about insertion and extraction watermark and in Section 5.3 we shown the results of segmentation of left ventricle in original and marked images. Finally, we conclude this study in Section 6.

2. HERMITE TRANSFORM

The Hermite transform (HT) is an image description model[17,18] that is obtained by performing a convolution of the image $L(x,y)$ with the filter functions $D_{m,n-m}(x,y)$:

$$L_{m,n-m}(x_0,y_0) = L(x,y) \otimes D_{m,n-m}(x,y) \tag{1}$$

where $L_{m,n-m}(x,y)$ are the Hermite coefficients, m and $(n-m)$ denote the analysis order in x and y direction respectively with $n = 0,1,\ldots,\infty$, $m = 0,1,\cdots,n$ and $D_{m,n-m}(x,y)$ are the Hermite filters which are determined by an analysis window $v^2(x,y)$ that expands the local information in terms of a family of polynomials $G_{m,n-m}(x,y)$.

Physiological experiments suggest using overlapping Gaussian windows separated by twice the standard deviation σ, in agreement with the overlapping receptive fields of the human visual system.[19] The polynomials that are orthogonal with respect to the Gaussian window function are defined by:

$$G_{m,n-m}(x,y) = \frac{1}{\sqrt{2^n m!(n-m)!}} H_m\left(\frac{x}{\sigma}\right) H_{n-m}\left(\frac{y}{\sigma}\right) \tag{2}$$

where H_n represents the generalized Hermite polynomials.

The Hermite filters $D_{m,n-m}(x,y) = D_m(x)D_{n-m}(y)$ are separable because the Gaussian window is rotationally symmetric and can be computed by:

$$D_n(x) = \frac{(-1)^n}{\sqrt{2^n n!}} \frac{1}{\sigma\sqrt{\pi}} H_n\left(\frac{x}{\sigma}\right) \exp\left(-\frac{x^2}{\sigma^2}\right) \tag{3}$$

In Fig. 1(left) we show the Hermite coefficients for the left ventricle of a cardiac CT image for $N = 3$ ($n = 0,1,\ldots,N$ and $m = 0,1,\cdots,n$).

The recovery process of the original image (inverse Hermite transform - IHT) consists of interpolating the Hermite coefficients through the proper synthesis filters:

$$\hat{L}(x,y) = \sum_{n=0}^{\infty} \sum_{m=0}^{n} \sum_{x_0,y_0 \in S} L_{m,n-m}(x_0,y_0) P_{m,n-m}(x-x_0, y-y_0) \tag{4}$$

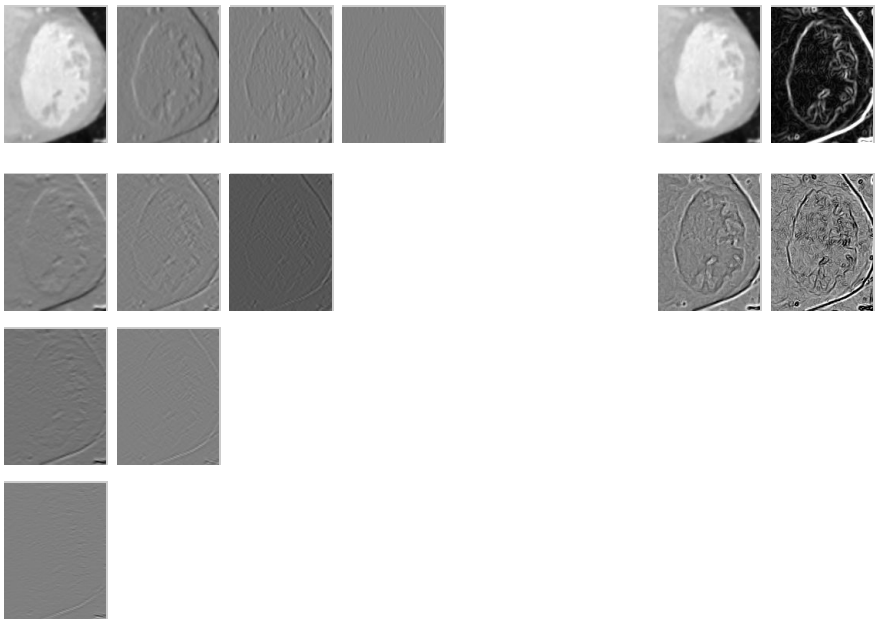

Figure 1. The Hermite coefficients $N = 3$ (left) for the left ventricle of a cardiac CT image $\begin{bmatrix} L_{0,0} & L_{1,0} & L_{2,0} & L_{3,0} \\ L_{0,1} & L_{1,1} & L_{2,1} & \\ L_{0,2} & L_{1,2} & & \\ L_{0,3} & & & \end{bmatrix}$. The steered Hermite coefficients $N = 3$ (right) $\begin{bmatrix} L_{0,0} & l_{1,\theta} \\ l_{2,\theta} & l_{3,\theta} \end{bmatrix}$.

where $P_{m,n-m}(x,y) = \frac{G_{m,n-m}(x,y)v^2(x,y)}{\sum_{(x_0,y_0)\in S} v^2(x-x_0,y-y_0)}$ for $m = 0,...,n$ and $n = 0,...,\infty$.

Steered Hermite filters belong to a class of filters that are rotated copies of each filter, constructed as a linear combination of a set of basis filters.[20] The orientation feature of the Hermite filters explains why they are products of polynomials with a radially symmetric window function (Gaussian function). The $N + 1$ Hermite filters of order n form a steerable basis for each individual filter of order n. Because of this characteristic, Hermite filters at each position in the image are adapted to local content.[21] The resulting filters can be interpreted as directional derivatives of a Gaussian function.

A steered version of Hermite transform is obtained by projecting the Hermite coefficients towards an orientation angle θ. The Hermite filters at each position in the image are projected to an angle given by the orientation of the local image feature:[21]

$$l_{m,n-m,\theta}(x_0,y_0) = \sum_{k=0}^{n} L_{k,n-k}(x_0,y_0)g_{k,n-k}(\theta) \tag{5}$$

where $g_{m,n-m}(\theta) = \sqrt{\binom{n}{m}}\left(\cos^m(\theta)\right)\left(\sin^{n-m}(\theta)\right)$ are the cartesian angular functions of order n that express the directional selectivity of the filter and $l_{m,n-m,\theta}(x_0,y_0)$ are the steered Hermite coefficients.

In order to obtain the steered Hermite coefficients, the Hermite coefficients are rotated toward the estimated local orientation, according to a criterion of maximum oriented energy at each window position. For local 1D patterns, the steered Hermite transform is an efficient way to compactly describe image features into a smaller number of coefficients ($l_{0,n,\theta}(x,y) = l_{n,\theta}(x,y)$) that represent the profile of the pattern perpendicular to its orientation (θ).[21]

In Fig. 1(right) we show the steered Hermite coefficients for the cartesian coefficients of Fig. 1(left).

3. WATERMARK ALGORITHM

The watermark method is inspired in the algorithm proposed by Ping, et al.[15] Originally, the algorithm uses the Discrete Cosine Transform (DCT) and to insert the watermark use spread spectrum method. Instead, we use the Hermite transform and include a perceptive mask in order to assure the invisibility of the mark. The process consist of:

1. The original image is normalized. A normalization procedure is aimed to transform an image and each of its affine transforms into a unique standard form, called the normalized image, and which meets a given set of image moment values. Therefore, normalization is a way to compensate for any affine geometric distortion and ensure invariance property to the normalized image.[15] We use the normalization parameters to normalize the perceptual mask (or template).
2. A binary pseudo random sequences is generated, as signature patterns using a private key as seed.
3. The alphanumeric code, such as patient's information, is convert to binary code, to use as watermark.
4. A watermark signature is created, modulating the watermark message with the patterns generated.
5. The watermark signature is converted into a 2D signature considering the watermarking strength.
6. Generate Hermite coefficients with null values. We assume that predefined Hermite sub-bands are watermarked. The watermark signature is inserted in those sub-bands. An inverse Hermite transform (IHT) is applied in order to obtained a watermark prototype.
7. A perceptive mask is built. The algorithm proposed by Ping et al.[15] originally uses a template of white pixels to generate the final watermark. We build our mask based on the argument that there is a reduced visual sensitivity to noise in high resolution bands, in areas with high or low brightness and in texture areas. We include a brightness model that considers the multichannel mechanism that the human vision system uses to build the psycho-physical perception of brightness.[22] Schouten indicated that brightness representation only depends on the objects properties, in other words, brightness is invariant to light source properties and the observation conditions. For the construction of the luminance-to-brightness map, Schouten divided the algorithm in three stages: scale representation, assembling the scaling signals and local adjustment of the brightness scale. The perceptive mask is then created using the brightness map and calculating the luminance masking from the Hermite approximation coefficients.[23] Finally the mask is normalized using the parameters obtained in step 1.
8. The final watermark is generated using the perceptive mask and the watermark prototype.
9. An inverse normalization procedure is applied to the final watermark so that it has the same size as the original image.
10. The final watermark is embedded into the original image additively.

In order to extract the watermark, we use a correlation detector. First we apply the normalization procedure to the watermark image. Then we decode the watermark message in the normalized image, as follows:

1. Regenerate the watermark patterns using the same key.
2. Apply the HT to the normalized image.
3. Convert the Hermite coefficient marked into a 1D vector.
4. Decode the alphanumeric watermark bit by bit, according to (Eq. 6):

$$Watermark = \begin{cases} 1 & \text{if } correlation = 0 \\ 0 & \text{otherwise} \end{cases} \tag{6}$$

4. SEGMENTATION METHOD

Deformable models and their implementation by level sets proposed in[24] have been widely used in medical image segmentation.[25] Deformable models rely on the idea that a curve from a given image, subject to some constraints, can evolve in order to detect objects. According to the image features used to handle the curve evolution, they can be categorized as edge based,[26] region based[27,28] and model shape based.[29,30] An extension of the method for vector-value images was proposed by Chan and Vese[31] and applied to color images. Additionally, Paraggios et al.[32] applied it to supervised texture segmentation problems. The vector value extension allows to introduce different kinds of features at the same time without requiring any prior knowledge. For example, Brox et al.[33] introduced simultaneously texture features, gray level and optic flow for the segmentation process.

To evaluate how the watermark algorithm modifies the visual information and the data content in marked images, we performed a segmentation using the Chan Vese vector-value image model.[31] The vector-value extension allows introducing different kinds of features at the same time without requiring any prior knowledge.

An important step in the algorithm is to construct the vector features. Different strategies are possible; one way is to take each vector component and apply a classical Gaussian kernel. However, the major problem with this approach is the attenuation of edges due to the smoothing of Gaussian Kernels that leads to an inaccurate results.

In this paper, we chose a nonlinear diffusion strategy for building the vector features that are introduced into the level set equation as in.[33] We introduced simultaneously gray level and steered Hermite coefficients for the nonlinear diffusion in the segmentation process as was presented in:[34]

$$\partial_t F_i = div\left(g\left(\sum_{k=1}^{\mathcal{N}}\left|F_k\right|^2\right)\nabla F_i\right) \qquad \forall i = 1,\cdots,\mathcal{N}. \tag{7}$$

where F is an evolving vector channel and $\mathcal{N}$ is the total number of vector channels. The joint diffusivity allows that an edge in one channel also inhibits smoothing in the others channels. For the initial condition $F := \left(L(x,y), l_{(n,\theta)}\right)$, where L(x,y) is the intensity of image and $l_{(n,\theta)}$ are the steered Hermite coefficients for $n = 0, ..., N$, with N as the order maximum of decomposition.

5. RESULTS

5.1 Materials

For our experiments, we used cardiac computed tomography studies from 2 patients. Such studies were performed on a CT Siemens dual source scanner with 128 channels. Each study contains 10 volumes that correspond to time percentage of the cardiac cycle divided by 10. None of them contain personal information.

The original volumes were aligned with the traditional short axis view by applying two spatial transformations using the Amira® software. The parameters of each transformation were obtained by visualizing the data volume and rotating the axial and the coronal axis.

5.2 Watermarking results

First we present the results on watermark insertion and extraction. Then we evaluated our method comparing the results obtained between perceptive mask and template. To identified the robustness algorithm we probe it with and without normalize process. We use two images from different patients at 0% of cardiac cicle (Fig. 2) and three different alphanumeric codes as watermark (80 bits, 104 bits and 140 bits).

To evaluate the algorithm performance we used two objective metrics by relating the original image L and the distorted image $\hat{L}$ both the same size $(X \times Y)$:

1. *PSNR* (Peak Signal to Noise Ratio in dB):

$$PSNR = 10\log_{10}\left(\frac{(\mathcal{M}-1)^2}{\frac{1}{XY}\sum_{X,Y}(L(i,j)-\hat{L}(i,j))^2}\right) \tag{8}$$

where $\mathcal{M}$ is the total number of gray levels of the image.

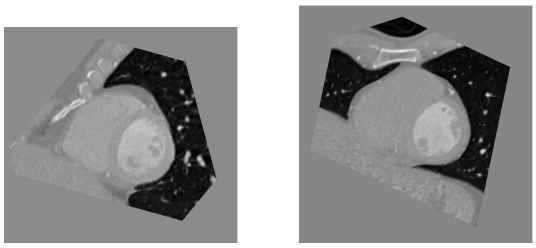

(a) Patient 1 (b) Patient 2

Figure 2. Patients' images.

Table 1. Metrics values using a template, and a perceptual mask with and without (Perceptual*) normalization process (patient 1).

Watermark	Normalization					
	Template		Perceptual		Perceptual*	
(bits)	PSNR [dB]	MSSIM	PSNR [dB]	MSSIM	PSNR [dB]	MSSIM
80	47.7055	0.9847	42.6609	0.9885	58.6617	0.9996
104	46.5680	0.9802	41.4967	0.9852	57.4961	0.9995
140	45.1338	0.9728	40.2018	0.9800	56.1818	0.9994

Table 2. Metrics values using a template, and a perceptual mask with and without (Perceptual*) normalization process (patient 2).

Watermark	Normalization					
	Template		Perceptual		Perceptual*	
(bits)	PSNR [dB]	MSSIM	PSNR [dB]	MSSIM	PSNR [dB]	MSSIM
80	43.7202	0.9663	41.9955	0.9870	57.6887	0.9996
104	42.5831	0.9568	40.8697	0.9836	56.5192	0.9994
140	41.1910	0.9419	39.4276	0.9777	55.0211	0.9992

2. *MSSIM* (Mean Structure Similarity Index) is given by Eq. 9:

$$MSSIM(L, \hat{L}) = \frac{1}{M} \sum_{j=1}^{M} SSIM(l_j, \hat{l}_j) \tag{9}$$

where $l_j, \hat{l}_j$ are the images contents at the *jth* local window and M is the number of local windows of the image. If $l, \hat{l}$ are two images with not negative values, *SSIM* is given by Eq. 10:

$$SSIM(l, \hat{l}) = \frac{(2\mu_l \mu_{\hat{l}} + C_1)(2\sigma_{l\hat{l}} + C_2)}{(\mu_l^2 + \mu_{\hat{l}}^2 + C_1)(\sigma_l^2 + \sigma_{\hat{l}}^2 + C_2)} \tag{10}$$

μ_l and $\mu_{\hat{l}}$ are their respective averages, σ_l, $\sigma_{\hat{l}}$ and $\sigma_{l\hat{l}}$ are the standard deviations and covariance, respectively. C_1 C_2 are constants to avoid instability when the denominator is close to zero.[35]

Table 1 shows the metric values using a template, and a perceptual mask with and without (Perceptual*) normalization process.

According to the results (Table 1), it is clear that better PSNR values are obtained using a template than using a perceptual mask with normalization. However, it is important that watermarked images do not differ perceptually from their originals, which can be assessed through the MSSIM metric. The best MSSIM value's are obtained using a perceptual mask.

In Table 2 we show the metrics values from patient 2.

In all cases the watermark was recovered successfully. The method without normalization process shows high PSNR and MSSIM values, which indicates that it is possible to embed and extract the watermark and the image will remain mostly unchanged.

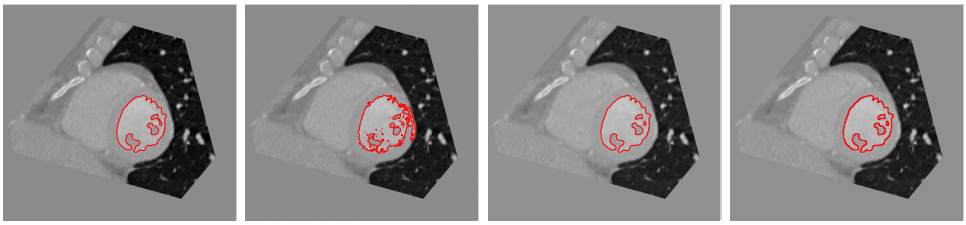

(a) (b) (c) (d)

Figure 3. Segmentation of left ventricle (patient 1) without mark (a) and segmentation with a 140-bit watermark and three different insertion masks: (b) template, (c) perceptual mask with normalization, and (d) perceptual mask without normalization.

Table 3. Dice index and Hausdorff distance for template and perceptual mask with and without (Perceptual*) normalization (patient 1).

Watermark	Normalization					
	Template		Perceptual		Perceptual*	
(bits)	Dice	Hausdorff	Dice	Hausdorff	Dice	Hausdorff
80	0.9891	3.6711	0.9956	1.1513	0.9961	**1.0840**
104	0.9888	3.1363	0.9951	1.1513	0.9956	**1.0920**
140	0.9291	48.0000	0.9947	**1.1171**	0.9949	1.1189

5.3 Segmentation results

In Fig. 3(a) we show the segmentation the original image (patient 1) without mark and in Fig. 3(b-d) the segmentation of watermark images with a 140-bit mark using a template and perceptual mask with and without normalization process respectively.

To evaluate the segmentation performance we use the Dice index and the Hausdorff distance. The Dice metric d_D is a measure of contour overlap between the segmentation reference (A) and the segmentation result (B) in the watermarked image:

$$d_D = \frac{2 \times (\|A \cap B\|)}{(\|A\| + \|B\|)} \tag{11}$$

The Dice value ranges between 0 and 1. Values close to 1 indicate more similar contours.

Moreover, the Hausdorff distance, d_H, measures how close a point from a reference set is from another point of the segmentation set in a metric space, in our case between two sets of points, P and Q (or boundaries). It is defined as follows:

$$d_H(P,Q) = \max\{d(P,Q),\, d(Q,P)\} \tag{12}$$

where $d(P,Q) = \min\{\|p_{max} - q\| \, |p_{max} \in \max\{\|p - q\|\}, q \subset Q, p \subset P\}$; intuitively, $d(P,Q)$ finds the p point from the set P that is the farthest from any point in Q and measures the distance from p to its closest neighbor in Q. Hausdorff minimal values indicate more alike boundaries in a range from 0 to 100.

For patient 1 we used as the reference set of points the segmentation result on original image without watermark and then we compared it with the watermarked images. In Table 3 we present the segmentation measures for a template and perceptual mask with and without normalization (Perceptual*) for patient 1.

In these results we noticed that both metrics show that the segmentation is not significantly different when using watermarks of different sizes. The Dice index gives values very close to 1 while Hausdorff distance generates very small values in most cases. Nevertheless using a perceptual approach, visual quality improves the segmentation in the marked images. It should be noted that using a template the Hausdorff distance increases considerably for large size marks.

In order to quantitatively evaluate the automatically detected endocardiadium, for patient 2 we computed the Dice index and Hausdorff distance using a manual segmentation by physician (Fig. 4(a)) where papillary muscles are included. In Fig. 4(b-d) we show the segmentation results using different mark sizes and the three mask insertion approaches.

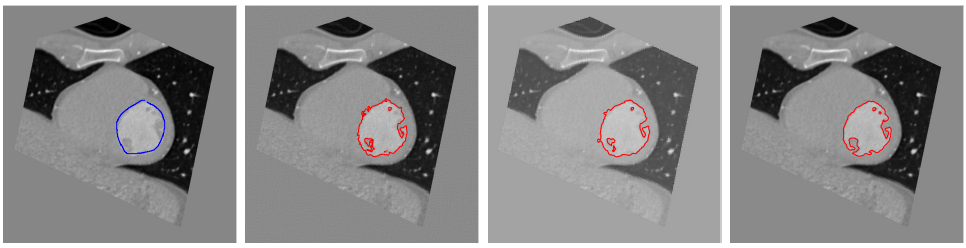

(a) (b) (c) (d)

Figure 4. Segmentation of left ventricle (patient 2) by physician (a) and segmentation with a 144-bit watermark and three different insertion masks: (b) template, (c) perceptual mask with normalization, and (d) perceptual mask without normalization.

Table 4. Dice index and Hausdorff distance for template and perceptual mask with normalization (patient 2).

Watermark	Normalization					
	Template		Perceptual		Perceptual*	
(bits)	Dice	Hausdorff	Dice	Hausdorff	Dice	Hausdorff
80	0.888	**31.575**	0.892	34.139	0.892	32.973
104	0.889	31.57	0.911	**27.893**	0.892	32.973
140	0.907	27.851	0.912	**27.659**	0.892	33.015

In Table 4 we present the segmentation measures for a template and perceptual mask with and without normalization.

The results in Table 4 show that approach perceptual with normalization is more robust that use a template or without normalization when we use large masks.

6. CONCLUSIONS

In this work, we have implemented a perceptive approach based on the Hermite transform to digital image watermarking using a brightness model and an image normalization applied to cardiac CT images. The Hermite transform is an image representation model that performs a decomposition of the images into relevant visual patterns and mimics some of the more important properties of early vision such as the behavior of retinal ganglion cell, e.g. local processing, and the Gaussian derivative models of receptive fields.

The proposed method allows inserting a perceptually invisible watermark using a brightness model to generate a perceptive mask and identify the image regions where the watermark detection becomes a difficult task for the human eye. In order to generate the mask, the following elements were considered: luminance to brightness map, contrast sensitivity and light adaptation threshold. We used the Hermite transform to embed the watermark into the transform coefficients of the original image.

In order to improve robustness against geometric attacks, we propose the use of image normalization techniques that transform the original image so that the orientation and the scale of the objects are fixed. For this purpose, we employ geometric moments and invariants. In order to determine the effectiveness of our algorithm, we tested the algorithm using a template of white pixels instead of a perceptual mask.

The PSNR and MSSIM metrics show that marked images using a perceptual mask preserve the visual information and do not differ perceptually from their originals. In all cases the watermark was successfully recovered. We performed tests with different mark sizes in order to evaluate the capacity of the proposed method to insert patient's information.

In order to evaluate the data integrity on the watermarked images and how the visual information is modified, we evaluated the segmentation performance on these images. We used the steered Hermite coefficients as texture descriptors into a vector-value level sets framework using a joint nonlinear anisotropic diffusion of the gray level and the steered Hermite coefficients. The Dice index and Hausdorff distance show that there is a closer correspondence in the segmented watermark images when using a perceptive mask, even when the size of the mark increases. In all cases the left ventricle was detected correctly.

ACKNOWLEDGEMENTS

Sandra Gomez-Coronel thanks to Instituto Politécnico Nacional, specially to Comité Técnico para el Otorgamiento de Becas de Estudio, Apoyos Económicos y Licencias con Goce de Sueldo COTEBAL, and Universidad Nacional Autónoma de México.

Jorge Brieva and Ernesto Moya-Albor would like to thank the Facultad de Ingeniería of Universidad Panamericana for all support in this work.

Boris Escalante-Ramírez gives a special thank to UNAM for PAPIIT grant IG100814.

The authors wish to thank to Enrique Vallejo M.D. of Hospital Angeles Pedregal (México) for the CT images that were presented in this paper and Jimena Olveres Montiel, PhD student of UNAM (México), for perform the short axis projections.

REFERENCES

[1] Pan, W., Coatrieux, G., Cuppens-Boulahia, N., Cuppens, F., and Roux, C., "Medical image integrity control combining digital signature and lossless watermarking," in [*Data Privacy Management and Autonomus Spontaneous Security*], *Lecture Notes in Computer Science* **5939**, 153–162, Springer Berlin Heidelberg (2010).

[2] Coatrieux, G., Chazard, E., Beuscart, R., and Roux, C., "Lossless watermarking of categorical attributes for verifying medical data base integrity," in [*Engineering in Medicine and Biology Society,EMBC, 2011 Annual International Conference of the IEEE*], 8195–8198 (2011).

[3] Ruanaidh, J. J. K. O., Dowling, W. J., and Boland, F. M., "Watermarking digital images for copyright protection," *IEEE Proceedings Vision, Image and Signal Processsing* **143**, 250–256 (1996).

[4] Unser, M. and Aldroubi, A., "A review of wavelets in biomedical applications," *Proceedings of the IEEE* **84**, 626–638 (1996).

[5] Nikolaidis, N. and Pitas, I., "Robust image watermarking in the spatial domain," *Signal Processing* **66**, 385–403 (1998).

[6] Van Schyndel, R., Tirkel, A., and Osborne, C., "A digital watermark," *IEEE International Conference on Image Processing* **2**, 86 –90 (1994).

[7] Kimpan, S., Lasakul, A., and Chitwong, S., "Variable block size based adaptive watermarking in spatial domain," *IEEE International Symposium on Communications and Information Technology* **1**, 374 – 377 (2004).

[8] Bazziz, N., "Adaptive watermarking schemes based on a redundant contourlet transform," *IEEE International Conference on Image Processing* **1**, I – 221–4 (2005).

[9] Zhou, H., Qi, C., and Gao, X., "Low luminance smooth blocks based watermarking scheme in DCT domain," *International Conference on communications, circuits and systems proceedings* **1**, 19–23 (2006).

[10] Wolfgang, R. B., Podilchuck, C. I., and Delp, E. J., "Perceptual watermarks for digital images and video," *Proceedings of the IEEE* **87**(7), 1108–1123 (1999).

[11] Barni, M., Bartolini, F., and Piva, A., "Improved wavelet-based watermarking through pixel-wise masking," *IEEE Transactions on Image Processing* **10**, 783–791 (2001).

[12] Wu, J. H. K., Chang, R., Chen, C., Wang, C., Kuo, T.-H., Moon, W. K., and Chen, D.-R., "Tamper detection and recovery for medical images using near-lossless information hiding technique," *Journal of Digital Image* **21**, 59–76 (2008).

[13] Coatrieux, G., Maitre, H., Sankur, B., Rolland, Y., and Collorec, R., "Relevance of watermarking in medical imaging," in [*Workshop of the Int. Telemedical Information Soc. IEEE EMBS Int. Conf. Information Technology Applications in Biomedicine*], 250–255 (2000).

[14] Zain, J. M., Baldwin, L. P., and Clarke, M., "Reversible watermarking for authentication of DICOM images," *Twenty-sixth Annual International Conference of the IEEE Engineering in Medicine and Biology Society* **2**, 3237 – 3240 (2004).

[15] Ping, D., Brankov, J. G., Galatsanos, N. P., Yang, Y., and Davoine, F., "Digital watermarking robust to geometric distortions," *IEEE Transactiones on Image Processing* **14**, 2140–2150 (2005).

[16] Alghoniemy, M. and Tewfik, A. H., "Geometric distortion correction through image normalization," *IEEE International Conference on Multimedia and Expo* **3**, 1291–1294 (2000).
[17] Martens, J.-B., "The Hermite Transform-Theory," *IEEE Transactions on Acoustics, Speech and Signal Processing* **38**(9), 1595–1606 (1990).
[18] Martens, J.-B., "The Hermite Transform-Applications," *IEEE Transactions on Acoustics, Speech and Signal Processing* **38**(9), 1607–1618 (1990).
[19] Sakitt, B. and Barlow, H., "A Model for the Economical Encoding of the Visual Image in Cerebral Cortex," *Biological Cybernetics* **43**(2), 97–108 (1982).
[20] Freeman, W. T. and Adelson, E. H., "The Design and Use of Steerable Filters," *IEEE Transactions on Pattern Analysis and Machine Intelligence* **13**, 891–906 (1991).
[21] Van Dijk, A. M. and Martens, J., "Image representation and compression with steered Hermite transforms," *Signal Processing* **56**(1), 1–16 (1997).
[22] Schouten, G., *Luminance-brightness mapping: the missing decades*, PhD thesis, Technische Universiteit Eindhoven (1993).
[23] Escalante-Ramírez, B., López, P., and Silvan, J. L., "Sar image classification with a directional-oriented discrete hermite transform and markov random fields," *IEEE International Geoscience and Remote Sensing Symposium* **6**, 3423–3425 (2003).
[24] Osher, S. and Paragios, N., [*Geometric Level Set Methods in Imaging,Vision,and Graphics*], Springer-Verlag New York Inc., Secaucus NJ USA (2003).
[25] Suri, J., Liu, K., Singh, S., Laxminarayan, S., Zeng, X., and Reden, L., "Shape recovery algorithms using level sets in 2-d/3-d medical imagery: a state-of-the-art review," *IEEE Transactions on Information Technology in Biomedicine* **6**(1), 8–28 (2002).
[26] Caselles, V., Kimmel, R., and Sapiro, G., "Geodesic active contours," *Int. J. Comput. Vision* **22**(1), 61–79 (1997).
[27] Chan, T. and Vese, L., "Active contours without edges," *IEEE Transactions on Image Processing* **10**(2), 266–277 (2001).
[28] Gao, S. and Bui, T., "Image segmentation and selective smoothing by using mumford-shah model," *IEEE Transactions on Image Processing* **14**(10), 1537–1549 (2005).
[29] Huang, C.-L., "Shape-based level set method for image segmentation," in [*Ninth International Conference on Hybrid Intelligent Systems*], **1**, 243–246 (2009).
[30] Kohlberger, T., Uzunbas, M. G., Alvino, C., Kadir, T., Slosman, D., and Funka-Lea, G., "Organ segmentation with level sets using local shape and appearance priors," in [*Medical Image Computing and Computer-Assisted Intervention (MICCAI)*], Yang, G.-Z., Hawkes, D., Rueckert, D., Noble, A., and Taylor, C., eds., *Lecture Notes in Computer Science* **5762**, 34–42, Springer Berlin Heidelberg (2009).
[31] Chan, T. F., Sandberg, B. Y., and Vese, L. A., "Active contours without edges for vector-valued images," *Journal of Visual Communication and Image Representation* **11**, 130–141 (2000).
[32] Paragios, N. and Deriche, R., "Geodesic active regions: A new framework to deal with frame partition problems in computer vision," *Journal of Visual Communication and Image Representation* **13**(1-2), 249–268 (2002).
[33] Brox, T., Rousson, M., Deriche, R., and Weickert, J., "Colour, texture, and motion in level set based segmentation and tracking," *Image and Vision Computing* **28**(3), 376–390 (2010).
[34] Olveres, J., Nava, R., Moya-Albor, E., Escalante-Ramírez, B., Brieva, J., Cristóbal, G., and Vallejo, E., "Texture descriptor approaches to level set segmentation in medical images," in [*Proc. SPIE 9138, Optics, Photonics, and Digital Technologies for Multimedia Applications III*], **9138**, 91380J–91380J–12 (2014).
[35] Wang, S., Bovik, A., Sheikh, H., and Simoncelli, E., "Image quality assessment: from error visibility to structural similarity," *IEEE Transactions on Image Processing* **13**, 600–612 (2004).